



Center for Scientific Computation And Mathematical Modeling

University of Maryland, College Park



A dynamic two-phase flow model of proton exchange membrane fuel cells

K. Kühn, M. Ohlberger, J. O. Schumacher, C. Ziegler, R. Klöfkorn

May 2003

CSCAMM Report 03-07

<http://www.cscamm.umd.edu/publications/>



CSCAMM is part of the
College of Computer, Mathematical &
Physical Sciences (CMPS)

A dynamic two-phase flow model of proton exchange membrane fuel cells

Karsten Kühn^{ab}, Mario Ohlberger^{cd}, Jürgen O. Schumacher^a,
Christoph Ziegler^a, Robert Klöfkorn^c

1 Abstract

A dynamic two phase flow model for proton exchange membrane (PEM) fuel cells is presented. The two dimensional along-the-channel model includes the two phase flow of water (gaseous and liquid) in the porous diffusion layers and in the catalyst layers, as well as the transport of the species in the gas phase. Moreover, proton and water transport in the membrane and the oxygen reduction reaction in the cathodic catalyst layer is accounted for. The discretisation of the resulting flow equations is done by a mixed finite element approach. Based on this the transport equations for the species in each phase are discretised by a finite volume scheme. The coupled mixed finite element/finite volume approach gives the spatially resolved water and gas saturation and the species concentrations. In order to describe the charge transport in the fuel cell the Poisson equations for the electrons and protons are solved by using Galerkin finite element schemes.

2 Introduction

Water management is crucial for the undisturbed operation of PEM fuel cells and for the optimisation of the power output. Flooding of the fuel cell due to water production blocks the gas transport towards the catalyst grains of the electrodes. On the other hand, a dehumidification of the membrane leads to a poor protonic conductivity. Consequently, an increase of resistive losses and a decrease of output power result from a low hydration state of the membrane [1, 2].

In general, the water content depends on the position in the PEM fuel cell. Furthermore, water is transported in both, the liquid and the gaseous phase. The local

^aFraunhofer Institut für Solare Energiesysteme, Heidenhofstr. 2, 79110 Freiburg, Germany

^bInstitut für Theoretische Physik, Technische Hochschule Aachen, D-52056 Aachen, Germany

^cAbteilung für Angewandte Mathematik, Universität Freiburg, Hermann-Herder-Str. 10, 79104 Freiburg, Germany

^dCenter for Scientific Computation And Mathematical Modeling, University of Maryland, 4127 CSIC Building, College Park, MD, 20742-3289, USA

humidity depends on a series of operating parameters as, for example, temperature, gas stoichiometries, pressure, and the electrical current production of the cell.

Mathematical models of PEM fuel cells have been presented by several authors. Springer et al. presented a PEM fuel cell model describing the water content of the Nafion 117 membrane as a function of the water vapour activity [2]. In this way, the dependency of the protonic conductivity of the membrane on its humidity was accounted for. A drag/diffusion model for the water transport through the membrane was introduced. An along-the-channel model for water and heat management of PEM fuel cells was published by Nguyen and White [3]. The model allows to predict the temperature and current distribution along the one dimensional flow channels on the anode and cathode side. A stationary two-dimensional along-the-channel model was presented by Gurau et al. [4]. Their one-phase model accounts for mass transport of gaseous species in all layers of the PEM fuel cell. The Navier-Stokes equations were solved in the gas channels. Moreover, the model includes the effect of heat transport in the gas channels and in the porous media. Multicomponent gas transport in the porous electrode of a PEM fuel cell with an interdigitated gas distributor structure was investigated by Yi and Nguyen [5]. Isothermal and stationary conditions were assumed.

In the context of direct methanol fuel cells an elaborated two phase flow model has recently been proposed by Divisek, Fuhrmann et al. [6]. Modelling of two-phase flow in the porous air cathode of a PEM fuel cell was attempted by Wang et al. [7]. The transport coefficients in the stationary numerical two-phase model are parameterised as functions of the liquid water saturation s_w . The important influence of the permeabilities for liquid and gas phases as functions of the liquid water saturation were considered. Moreover, the capillary pressure-saturation relationship is included in the model allowing to study the influence of the contact angle between the liquid and the solid phase.

The modelling approach of our present work is based on a two phase flow formulation for arbitrary porous media introduced in [8]. Locally distributed flooding effects can be described by the model in detail because the model accounts separately for the gaseous and the liquid water transport. Therefore, the influence of material parameters influencing the water transport on the fuel cell performance can be studied. The model accounts for the time dependent transport equations and for the kinetics of the electrochemical reaction. Therefore, flooding and drying effects can be investigated dynamically.

3 Development of the dynamic two-phase flow model

The modelling domain is shown in Fig. 1 representing a cross-section along the parallel channels of an along-the-channel test fuel cell. It is assumed that the channels on the anode and cathode side appear in the same cross-section. The cell

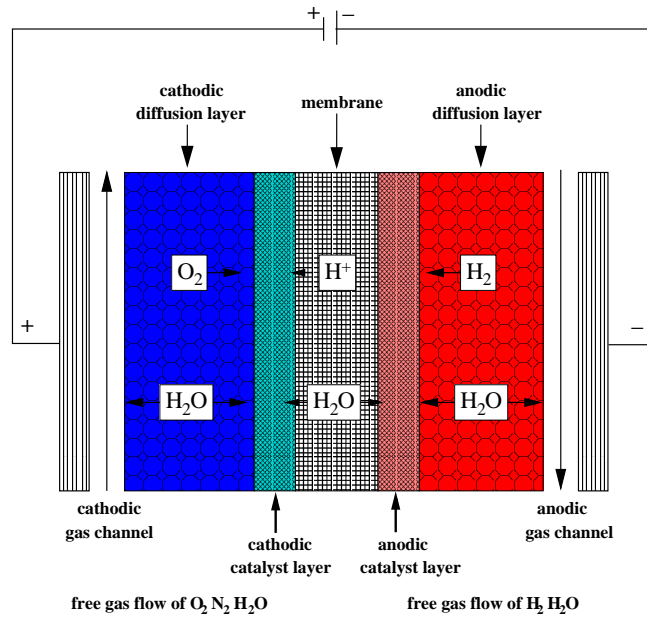


Figure 1: Modelling domain of the along-the-channel fuel cell.

dimensions are $2000 \mu m$ vertical and $450 \mu m$ horizontal. An anisotropic scaling of the transport equations is needed in order to describe channel lengths in the centimeter range. Along the channel we assume a pressure decrease in flow direction with a negative constant gradient. We can choose the inlet/outlet pressure difference and switch the gas flow direction between co- and counterflow (parallel and anti-parallel).

Furthermore, the following simplifying assumptions have been considered in the model:

1. In a PEM fuel cell water is dragged from the anode to the cathode side by interaction of protons with the water molecules in the membrane [2]. Water transport through the membrane due to the electroosmotic drag was neglected so far.
2. A proton exchange membrane exhibits a strong dependence of the protonic conductivity on the water content of the membrane. The proton conductivity of the membrane is assumed to be constant in the present work.
3. Hydrophilic pores of a membrane made of Nafion appear as a result of their contact with water. These pores collapse after water removal in the process of drying [9]. Consequently, the permeability of a proton exchange membrane depends on its water content. A constant membrane permeability K is assumed here.
4. Heat transport is not taken into account in the current implementation of the

model. Isothermal conditions are assumed to be valid (i.e. the cell is operated at constant temperature).

5. The exchange current density for the oxygen reduction reaction is assumed to be independent of the temperature.
6. Diffusion of the gas components is modelled according to Fick's law. Multi-component diffusion has not been considered here.
7. Double layer charging is not accounted for.

Note that the model is not in general limited to these restrictions, but will be relaxed step by step in the framework of our current implementation.

3.1 Governing differential equations

The mass balance equations for both, the liquid and the gaseous phase in the porous media can be written as follows [8]

$$\partial_t(n\rho_i s_i) + \nabla \cdot (\rho_i \mathbf{v}_i) = q_i \quad (1)$$

$$\mathbf{v}_i = -K \frac{k_{ri}}{\mu_i} \nabla p_i. \quad i = w, g. \quad (2)$$

where n is the porosity, ρ_i is the mass density and s_i is the saturation of phase i . Saturation means the volume fraction of the phase within the pore space. Furthermore, v_i is the Darcy-velocity and p_i is the pressure in the i -th phase. The index $i = w, g$ denotes the liquid and the gaseous phases, respectively.

The source term q_i is expressed by Eq. (12). The following supporting equations are used

$$s_w + s_g = 1, \quad (3)$$

$$p_g - p_w = p_c(s_w), \quad (4)$$

$$\rho_i = \rho_i(T, p_i), \quad (5)$$

where $p_c(s_w)$ is the capillary pressure-saturation function. It depends on the interfacial tension between the liquid water and the solid phase of the porous zone. Moreover, $p_c(s_w)$ is determined by the pore geometry. A parameterisation of the $p_c(s_w)$ -relationship is given by the Van Genuchten model [8].

Water is the only species of the liquid phase and therefore no transport equation has to be solved for water within the liquid phase, whereas hydrogen, oxygen, water vapour and nitrogen are present in the gas phase of a hydrogen PEM fuel cell. Therefore transport equations for each species in the gaseous phase have to be solved. Species in the gaseous phase are referred to as $k = H_2, O_2, H_2O$. The following supporting equation for the mass fractions c^k of the gas components holds

$$c^{H_2} + c^{O_2} + c^{H_2O} + c^R = 1, \quad (6)$$

where R refers to nitrogen as the inertial rest gas. Transport of the gaseous components are modelled separately

$$\partial_t(n\rho_g s_g c^k) + \nabla \cdot (\rho_g \mathbf{v}_g c^k) - \nabla \cdot (n\rho_g s_g D_g^k \nabla c^k) = q_g^k, \quad (7)$$

where D_g^k is the diffusivity of the k -th species. The source terms q_g^k of the gaseous components are determined by the electrochemical reactions occurring in the electrodes (Eqs. (16)-(18)).

Finally, the flow of electrons and protons ($l = e, p$) is governed by the potential equations

$$\nabla \cdot \mathbf{j}_l = q_l \quad (8)$$

$$\mathbf{j}_l = -\sigma_l \nabla \Phi_l, \quad (9)$$

where Φ_l is the potential of the charge carrier and j_l is the current density. The protonic conductivity of the PEM depends on its water content, that is $\sigma_p = \sigma_p(s_w)$ [2]. The electrochemical reactions represent the source terms q_l of the potential equations (Eqs. (14), (15), (19), (20)).

3.2 Source terms and coupling of the differential equations

The phase transition of water between the liquid and the gaseous phase is modelled according to Nguyen [10]

$$q_w = r_{\text{phase}}, \quad (10)$$

$$q_g = -r_{\text{phase}}, \quad (11)$$

$$\begin{aligned} r_{\text{phase}} := & k_c n s_g \frac{M_g (\rho_{g,w} - \rho_w^{\text{sat}}) c_{H_2O}}{R T} \text{sgn}(\rho_{g,w} - \rho_w^{\text{sat}}) \\ & + k_v \rho_s (\rho_{g,w} - \rho_w^{\text{sat}}) \text{sgn}(\rho_w^{\text{sat}} - \rho_{g,w}) \end{aligned} \quad (12)$$

The first term of Eq. (12) represents the condensation of water, where k_c is the condensation rate constant and M_g is the average molar mass of the gas phase. The second term represents the evaporation of water with the evaporation rate constant k_v . The saturation density of liquid water depends on the water saturation s_w

$$\rho_s = s_w n \rho_w, \quad (13)$$

where ρ_w is the density of liquid water. Water condenses if the partial pressure $\rho_{g,w}$ of water vapour is higher than the water saturation pressure ρ_w^{sat} .

The kinetics of the electrochemical reactions in the electrodes can be approximated using the Tafel approach [11]

$$r_c = -(1-n) a i_{0,c} \frac{[O_2]^s}{[O_2]_{\text{ref}}} \exp\left(-\frac{2\alpha F}{RT} (\Phi_e - \Phi_p - \Delta\Phi_c^{\text{ref}})\right), \quad (14)$$

$$r_a = (1-n) a i_{0,a} \frac{[H_2]^s}{[H_2]_{\text{ref}}} \exp\left(\frac{\alpha F}{RT} (\Phi_e - \Phi_p - \Delta\Phi_a^{\text{ref}})\right), \quad (15)$$

where n is the electrode porosity and $i_{0,c}$ and $i_{0,a}$ are the exchange current density of the oxygen reduction reaction $O_2 + 4e^- + 4H^+ \rightarrow 2H_2O$ in the cathode and the hydrogen oxidation reaction $H_2 \rightarrow 2H^+ + 2e^-$ in the anode at reference conditions, respectively. Furthermore, $\Delta\Phi_{a,c}^{ref}$ is the difference of electrical potential between the electrode and membrane phases at equilibrium conditions. r_a and r_c can be interpreted as the generation rates of positive charge carriers per unit electrode volume. It is assumed that the specific surface area a of the catalyst particles per unit electrode volume is equal on both, the anode and cathode side. The source terms of the gaseous components, q_g^k in Eq. (7), are related to the ionic current density in the electrodes by Faraday's law

$$q_g^{H_2} = \begin{cases} -\frac{M_{H_2}}{2F} r_a & \text{in the anodic catalyst layer} \\ 0 & \text{in the cathodic catalyst layer} \end{cases}, \quad (16)$$

$$q_g^{O_2} = \begin{cases} 0 & \text{in the anodic catalyst layer} \\ \frac{M_{O_2}}{4F} r_c & \text{in the cathodic catalyst layer} \end{cases}, \quad (17)$$

$$q_g^{H_2O} = \begin{cases} q_g & \text{in the anodic catalyst layer} \\ -\frac{M_{H_2O}}{2F} r_c + q_g & \text{in the cathodic catalyst layer} \end{cases}. \quad (18)$$

Eq. (18) contains the water production term $-\frac{M_{H_2O}}{2F} r_c$ due to the oxygen reduction reaction on the cathode side. We assume here that water is produced in the gaseous phase.

The source terms of the potential equations (Eq. (9)) are

$$q_e = \begin{cases} -r_a & \text{in the anodic catalyst layer} \\ -r_c & \text{in the cathodic catalyst layer} \end{cases}, \quad (19)$$

$$q_p = \begin{cases} r_a & \text{in the anodic catalyst layer} \\ r_c & \text{in the cathodic catalyst layer} \end{cases}. \quad (20)$$

3.3 Parameters and boundary conditions

Along the gas flow channels on the cathode and the anode side, the boundary conditions are specified as a linear pressure drop along the channel. This assumption is valid if the gas transport in the gas channels is not blocked by water droplets in the liquid phase.

Initially no liquid water is assumed to be present. Moreover, the boundary conditions at the gas inlets were also set to $s_w = 0$.

The initial and boundary conditions are adjusted for saturated atmosphere according to Fig. 2

$$x_{H_2O}^{sat} = \frac{p_w^{sat}}{p_{gas}} \quad (21)$$

$$c_{H_2O}^{sat} = \frac{M_{H_2O}}{M_g} x_{H_2O}^{sat}. \quad (22)$$

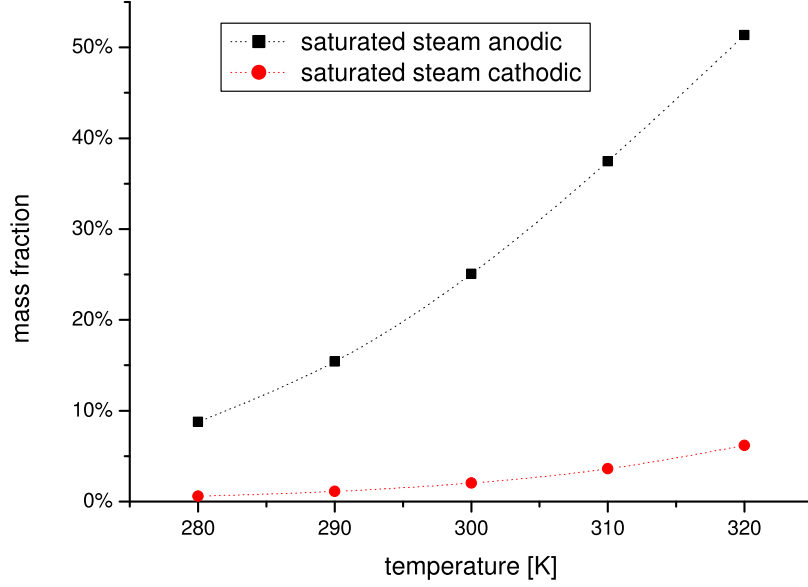


Figure 2: Saturated steam mass fraction

with

$$\begin{aligned}
 p_w^{\text{sat}}(T_c) &= 10^{-\alpha + \beta T_c - \gamma T_c^2 + \delta T_c^3} \cdot 10^5 \text{ Pa} & (23) \\
 \alpha &= 2.18; \\
 \beta &= 2.95 \cdot 10^{-2} \text{ K}^{-1} \\
 \gamma &= 2.95 \cdot 10^{-5} \text{ K}^{-2} \\
 \delta &= 1.44 \cdot 10^{-7} \text{ K}^{-3} \\
 T_c &= \frac{T - 273.13 \text{ K}}{K} \text{ } ^\circ \text{C}
 \end{aligned}$$

Simulation results discussed in the following are obtained at a temperature of $T = 290 \text{ K}$.

The Tafel slope of the oxygen reduction reaction was extracted from steady state voltammograms. From this the cathodic transfer coefficient (symmetry factor) was calculated: $\alpha = \frac{RT}{z_c \xi_c F}$, where $z_{a/c}$ is the number of electrons involved in one reaction step, anodic and cathodic, respectively. $\xi_{a/c}$ is the anodic or cathodic Tafel slope with the natural base e in contrast to the decade Tafel slope $b = 2.3\xi$.

4 Discretisation of the governing equations

The discretisation of the two phase flow equations (1) and (2) is based upon an equivalent global pressure formulation (for details see [12, 13, 14]). The resulting system of equations consists of an elliptic equation for a global pressure, coupled with a weakly degenerate parabolic equation for the water saturation. The discretisation of these equations is done by using Raviart-Thomas mixed finite elements

Table 1: Parameters determining the mass transport

Parameter	Symbol	Value
porosity of gas diffusion layer (GDL)	n	0.8
electrode porosity	n	0.4
membrane porosity	n	0.001
permeability of gas diffusion layer (GDL)	K	$2 \cdot 10^{-11} \text{ m}^2$
electrode permeability	K	$1 \cdot 10^{-12} \text{ m}^2$
membrane permeability	K	$1 \cdot 10^{-14} \text{ m}^2$
diffusivity	D_g^k	$1.4 \cdot 10^{-8} \text{ m}^2 \cdot \text{s}^{-1}$
condensation rate constant	k_c	$1 \cdot 10^3 \text{ s}^{-1}$
vapourisation rate constant	k_v	$1 \cdot 10^{-4} (\text{Pa} \cdot \text{s})^{-1}$

Table 2: Parameters of the electrochemical reactions

Parameter	Symbol	Value
exchange current density (O_2 -reduction)	$i_{0,c}$	1 A m^{-2}
exchange current density (H_2 -oxidation)	$i_{0,a}$	$1 \cdot 10^4 \text{ A m}^{-2}$
specific surface area	a	$1 \cdot 10^7 \text{ m}^2 \text{ m}^{-3}$
equilibrium potential difference (cathode)	$\Delta\Phi_c^{ref}$	1 V
equilibrium potential difference (anode)	$\Delta\Phi_a^{ref}$	0 V
transfer coefficient (cathode)	α	0.11

for the pressure equation and a semi-implicit cell centered finite volume scheme for the saturation equation. In order to achieve efficiency of the method a fully self adaptive grid refinement is used which is based on rigorous a posteriori error estimates for both, the mixed finite element approximation and the finite volume scheme. Details of these adaptive methods were presented in [15, 14].

Having solved for the global pressure and the global velocity field, the transport velocities in the water and gas phases respectively are recomputed (see [12]).

The reactive transport equations for the species in the gas phase (7) are discretised again by using a self adaptive finite volume scheme based on rigorous a posteriori error estimates for so called weakly coupled systems. For details we refer to [16, 17, 18, 19].

Finally, these transport equations are coupled to the potential equations for the proton and electron flow (9) through the reactive source terms. The potential equations are solved by a Galerkin finite element method using standard piecewise linear basis functions. In order to cope with the strongly non linear source term, a time relaxation of the stationary potential equations is used. This time stepping approach also incorporates a non-linear fixed point iteration for the solution of the resulting non-linear coupled system.

A detailed description of the resulting overall algorithm is beyond the scope of this contribution and will be presented in a forthcoming paper.

5 Numerical simulation results

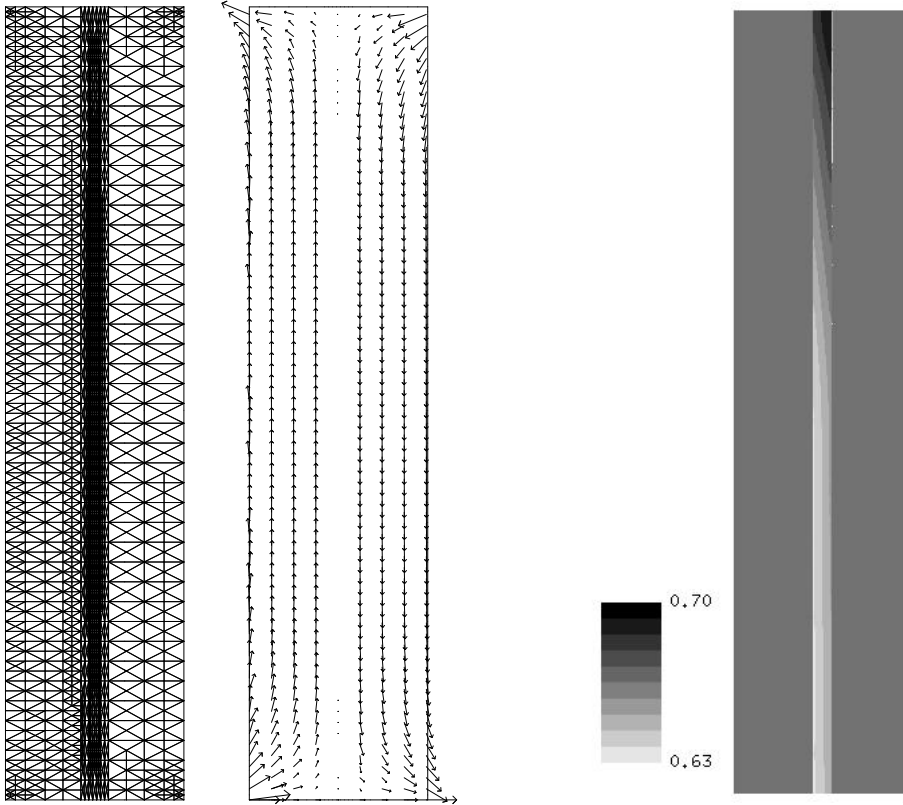


Figure 3: grid and velocity field at $t = 3s$ Figure 4: protonic potential $\phi_e[V]$

The adaptively refined discretisation mesh of the modelling domain (Fig. 1) is shown on the left hand side of Fig. 3. At simulation time $t = 3s$ a refinement of the triangulation can be seen in the corners of the domain. This is due to the high velocity values at the gas inlet and outlet. The grid is also refined in the electrodes where the electrochemical reactions occur. An adaptive grid refinement is realised in order to handle the high potential gradients in these regions. Such a spatially resolved protonic potential Φ_p is shown in Fig. 4. The global velocity field in the porous gas diffusion layers is shown on the right hand side of Fig. 3 corresponding to the case of counterflow. Absolute values of the global velocity in the membrane are three orders of magnitude lower compared to the gas diffusion layers. According to Eq. (2) this reduction is determined by the decrease of permeability listed in Table 1.

The protonic potential along a cut-line through the membrane electrode assembly is shown on the left hand side of Fig. 6. At the boundary between the catalyst layers

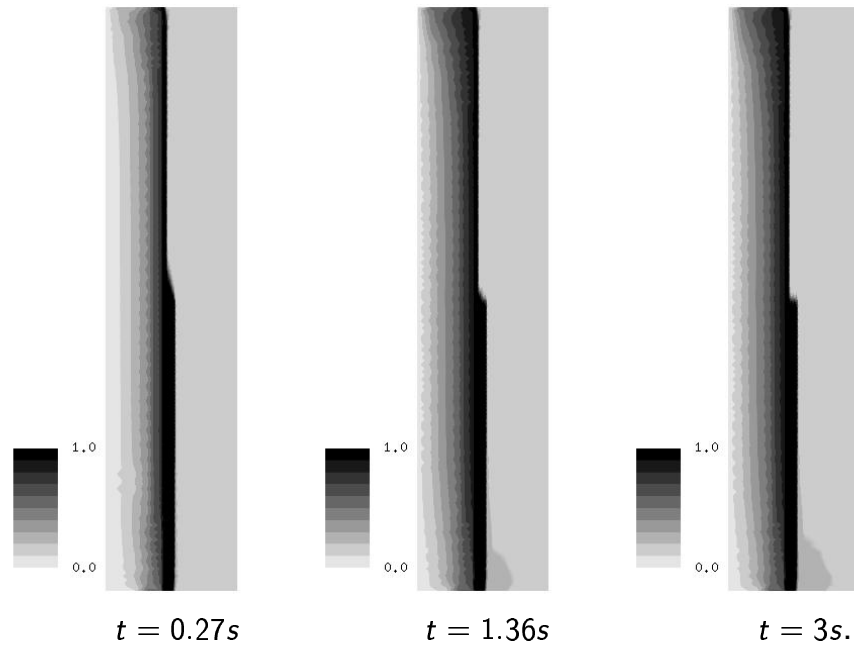
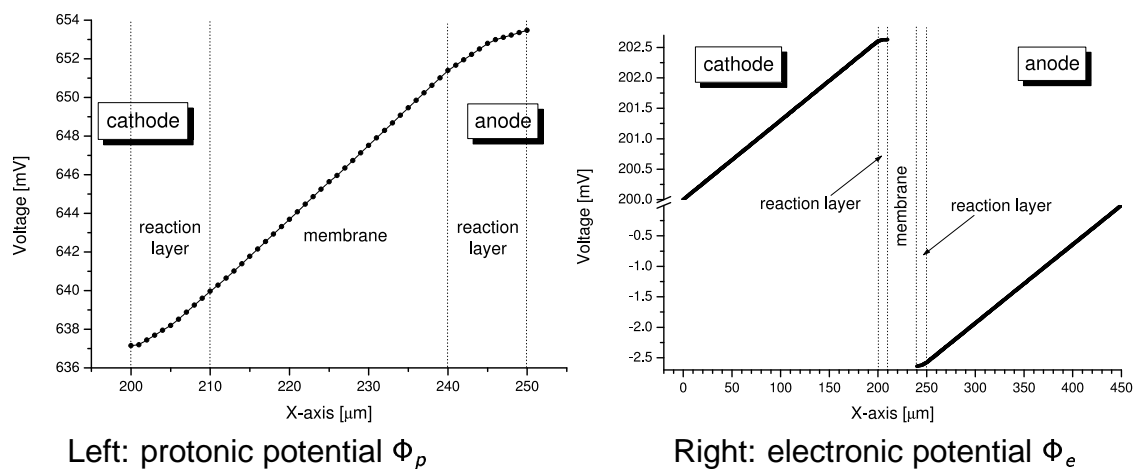


Figure 5: The local distribution of the mass fraction of water vapour is shown.

and the gas diffusion layers the gradient of the protonic potential is zero, i.e., there is no protonic current in the gas diffusion layers. In the membrane the gradient of the protonic potential is constant due to the ohmic drop. The electronic potential Φ_e is shown on the right hand side of Fig. 6. It is defined in the gas diffusion layers and the catalyst reaction layers. Here the constant values of the gradients appear in the gas diffusion layers. The membrane is an electronic insulator, therefore the electron potential gradient at the boundary to the membrane is zero.

The local distribution of the mass fraction of water vapour can be seen in Fig. 5. Note that at saturated atmosphere the colours vary on the anode and cathode side in consequence of using mass fractions instead of molar fractions. We assume that



Left: protonic potential Φ_p

Right: electronic potential Φ_e

Figure 6: Cross sections of the electric potentials at simulation time 0.27 s.

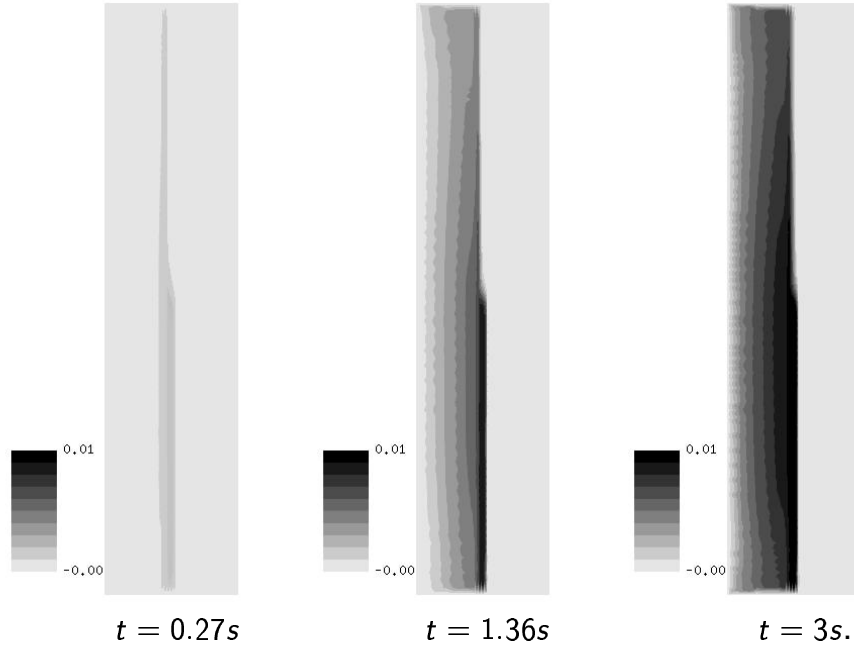


Figure 7: The local distribution of the liquid water saturation s_w is shown.

water production due to the electrochemical reaction on the cathode side occurs in the gaseous phase. Therefore, maximum values of the water vapour mass fraction can be found in the electrode of the cathode side. Water vapour is accumulated in the membrane which is due to the small flow velocity in this region. A comparison between three subsequent simulation times is shown revealing an increase of the water vapour mass fraction on the cathode side. A small amount of vapour diffuses to the anode side. The time evolution of the water vapour distribution is determined by the velocity field. On both, the anode and cathode side, the gas flow carries away the water vapour in flow direction.

The local distribution of the liquid water saturation s_w is shown in Fig. 7. A comparison between three subsequent simulation times is shown revealing an increase of the liquid water values on the cathode side according to the water vapour production in Fig. 5. Liquid water accumulates in the center of the cathode reaction layer. At the anode side no liquid water occurs. Liquid water is produced due to the phase transition during the simulation period because the water vapour pressure $p_{g,w}$ in our simulation exceeds the water saturation pressure p_w^{sat} at $T = 290K$. After about 4 seconds the condensation rate of water vapour to liquid approaches an equilibrium value. In this equilibrium state further production of vapour will lead to condensation of the corresponding amount of water. Water vapour at boiling temperature has a density of only $0.768 \frac{kg}{m^3}$ corresponding to less than 1 per mill volumetric content when condensed to liquid. At lower temperatures the contribution is even lower, hence the water production is basically governed by the electrochemical reaction. According to the reaction rate flooding of a cell is a process on a time scale of minutes.

Fig. 8 shows the water saturation in a sequence of cross sections perpendicular

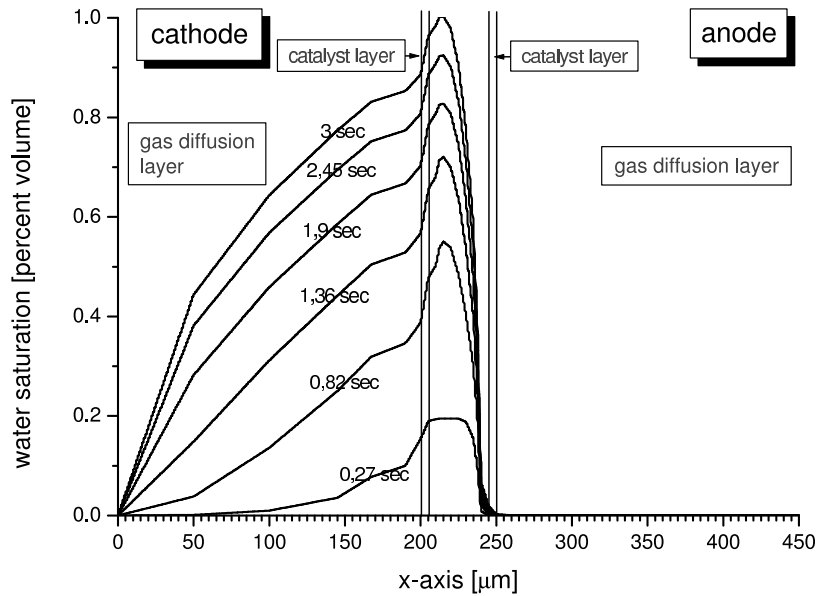


Figure 8: The liquid water saturation s_w is shown along a cut line through the gas diffusion layer and membrane-electrode-assembly.

to the membrane. The saturation increases with time. The maximum increase is near the cathodic catalyst layer and the highest gradient forms in the middle of the membrane. The increase of saturation attenuates with time. According to Fig. 7 there is no liquid water present at the anode side.

6 Conclusion and outlook

The present work demonstrates that a dynamic two-phase flow model of a proton exchange membrane fuel cell can be set up using state-of-the-art numerical methods. Our present model accounts for the following physical and electrochemical phenomena which govern the PEM fuel cell performance: the mass-transport of water in both, the liquid and the gaseous phase, the electrochemical reaction of oxygen and hydrogen and the flow of protons and electrons. Dynamic effects in a PEM fuel cell on a time scale of several seconds can be studied. We introduced a number of simplifying assumptions which are discussed in detail in Section 3. Note that the model is not in general limited to these restrictions, but will be relaxed step by step in the framework of our current implementation. Having implemented more details of the membrane water transport properties various problems can be approached which are beyond the scope of commercially available stationary one-phase models:

- The influence of hydrophilic and hydrophobic porous regions on the time dependent water distribution can be studied. This is essential for efficient water management of a PEM fuel cell.

- The local distribution of membrane humidification can be investigated for different operating conditions.
- The cell response on a change in the operating conditions can be studied dynamically. For example, the change in the reactant distribution on a step of the cell voltage can be simulated.
- With improved time step control of the numerical solution procedure a simulation period of minutes can be reached. Then locally distributed flooding effects can be investigated. Moreover, drying effects of the membrane and catalyst layers and mass transport problems of the reaction gases to the catalyst layers can be studied.

References

- [1] T. E. Springer, T. A. Zawodzinski, S. Gottesfeld, Modeling water content effects in polymer electrolyte fuel cells, in: R. E. White, M. W. Verbrugge, J. F. Stockel (Eds.), Modelling of batteries and fuel cells, Vol. 91-10, The Electrochemical Society, Softbound Proceedings Series, Pennington, NJ, 1991, pp. 209–223.
- [2] T. E. Springer, T. A. Zawodzinski, S. Gottesfeld, Polymer electrolyte fuel cell model, *J. Electrochem. Soc.* 138 (8) (1991) 2334–2342.
- [3] T. V. Nguyen, R. E. White, A water and heat management model for proton-exchange-membrane fuel cells, *J. Electrochem. Soc.* 140 (8) (1993) 2178–2186.
- [4] V. Gurau, H. Liu, S. Kakac, Two-dimensional model for proton exchange membrane fuel cells, *AIChE Journal* 44 (11) (1998) 2410–2422.
- [5] J. S. Yi, T. V. Nguyen, Multicomponent transport in porous electrodes of proton exchange membrane fuel cells using the interdigitated gas distributors, *J. Electrochem. Soc.* 146 (1) (1999) 38–45.
- [6] J. Divisek, J. Fuhrmann, K. Gärtner, R. Jung, Performance modeling of direct methanol fuel cells, Tech. rep., submitted (2002).
- [7] Z. H. Wang, C. Y. Wang, K. S. Chen, Two-phase flow and transport in the air cathode of proton exchange membrane fuel cells, *Journal of Power Sources* 94 (2001) 40–50.
- [8] R. Helmig, *Multiphase Flow and Transport Processes in the Subsurface: A contribution to the modeling of hydrosystems*, Springer, Berlin, Heidelberg, 1997.

- [9] M. Eikerling, Y. I. Kharkats, A. A. Kornyshev, Y. M. Volfkovich, Phenomenological theory of electro-osmotic effect and water management in polymer electrolyte proton-conducting membranes, *J. Electrochem. Soc.* 145 (8) (1998) 2684–2699.
- [10] T. Nguyen, Modeling of two-phase flow in the porous electrodes of proton exchange membrane fuel cells using the interdigitated flow fields, *Tutorials in Electrochem. - Engineering Mathem. Modeling; The Electrochemical Society Proceedings 99-14* (1999) 222–241.
- [11] A. Bard, L. Faulkner, *Electrochemical methods*, John Wiley and Sons, New York, 1980.
- [12] Z. Chen, R. Ewing, E. M.S., Multiphase flow simulation with various boundary conditions, in: P. et al. (Ed.), *Computational Methods in Water Resources*, Kluwer Academic Publishers, Netherlands, 1994, pp. 925–932.
- [13] M. Ohlberger, Convergence of a Mixed Finite Element - Finite Volume Method for the Two Phase Flow in Porous Media, *East-West J. Numer. Math.* 5 (1997) 183–210.
- [14] D. Bürkle, M. Ohlberger, Adaptive finite volume methods for displacement problems in porous media, *Comput. Visual. Sci.* 5 (2) (2002) 95–106.
- [15] M. Ohlberger, Adaptive mesh refinement for single and two phase flow problems in porous media, in: *Proceedings of the 2nd International Symposium on: FINITE VOLUMES FOR COMPLEX APPLICATIONS - PROBLEMS AND PERSPECTIVES*, Duisburg (1999), Hermes Science Publications, Paris, 1999, pp. 761–768.
- [16] R. Herbin, M. Ohlberger, A posteriori error estimate for finite volume approximations of convection diffusion problems, in: *Proceedings of the 3rd International Symposium on: FINITE VOLUMES FOR COMPLEX APPLICATIONS - PROBLEMS AND PERSPECTIVES*, Porquerolles (2002), Hermes Science Publications, Paris, 2002, pp. 753–760.
- [17] M. Ohlberger, C. Rohde, Adaptive finite volume approximations for weakly coupled convection dominated parabolic systems, *IMA J. Numer. Anal.* 22(2) (2002) 253–280.
- [18] R. Klöforn, D. Kröner, M. Ohlberger, Local adaptive methods for convection dominated problems, *Internat. J. Numer. Methods Fluids* 40 (1-2) (2002) 79–91.
- [19] M. Ohlberger, Higher order finite volume methods on selfadaptive grids for convection dominated reactive transport problems in porous media., Preprint 02-25, Mathematische Fakultät, Universität Freiburg (2002).